A first attempt at assimilating microwave-derived SST to improve the predictive capability of a coupled, high-resolution Eta-POM forecasting system.

C. Galdies† and D. N. M. Donoghue‡

† Euro-Mediterranean Centre on Insular Coastal Dynamics, Malta;
now at: National Meteorological Services, Malta International Airport, Luqa, Malta

‡Dept. of Geography, University of Durham, Department of Geography Science Laboratories, South Road, Durham, DH1 3LE, UK

Abstract

This study implements the assimilation of sea surface temperature (SST) data acquired by passive microwave remote sensing to a high-resolution, primitive-equation ocean model. The aim was to improve a forecasting tool capable of predicting the surface ocean processes linked to the air-sea interactions at sub-mesoscale level using one-way coupled, atmosphere-ocean modelling. An assimilation scheme based on a Newtonian relaxation scheme was fine-tuned to improve the forecasting skill of the ocean model. The ocean model was driven by predicted, synchronous air-sea fluxes derived by an overlying atmosphere model, remotely sensed SST and lateral boundary conditions derived from its previous run. The estimation of the model forecasting error was based on statistical and spatial comparison with remotely sensed observations. The optimal nudging coefficient was found to be $5x10^{-4}$ for 12 hours, giving a mean bias of –0.07 ^{o}C. Forecast validation was done against calibrated AVHRR scenes using a new approach to calibrate region-specific scenes based on the split-window technique. This work demonstrates the benefit of using passive microwave remote sensing to improve high-resolution, ocean forecasting systems. It also shows the high complementarity of infrared and passive microwave satellite sensors to provide information on the surface thermodynamics of the Ionian Sea.

1. Introduction

The progress of ocean forecasting is still hindered by a number of constraints. Chassignet *et al.* (2004) identified one of the main constraints as being due to uncertainties of the boundary and initial conditions of the ocean model. According to the World Ocean Circulation Experiment, scientific progress in data assimilation is still at an early stage of development by the oceanographic community, and its eventual success will be important to the ocean forecasters in general. Data assimilation, which is the incorporation of observations into a mathematical model to improve the initialisation of dynamical models, is a versatile methodology that makes efficient, accurate and realistic estimation of initial model conditions possible (Robinson and Lermusiaux, 2001). The initial and boundary conditions necessary for integration of the equations of an ocean model (i.e. velocity components, pressure, density, temperature and salinity) are very often difficult, if not impossible, to measure because of high sampling, technical and resource requirements. Using model numerics however, data assimilation adjusts these fields according to their physical relation with the independent, realistic observations.

One form of assimilation method is known as dynamical forced adjustment, and a good example of this is known as Newtonian relaxation (Hoke and Anthes, 1976). This approach is widely applied in regional scale models and consists of replacing forecast values by observed ones, at all data points. The *a priori* hypothesis is that the observations are exact. The blending

estimate is a scalar linear combination of the forecast and data values at all data points, with user assigned weights. Newtonian relaxation provides field balancing during a full-model pre-forecast integration. This is done by adding the correction terms in the prognostic equations (by means of a nudging coefficient), thus forcing the model fields toward the target analysis as defined by the observations (Robinson and Lermusiaux, 2001). The final state is the result of both model adjustment mechanisms as well as the observed information.

Ocean surface temperature is one of the most significant boundary conditions for the general circulation of the atmosphere, important prognostic ocean model field and a model output of primary interest. For these reasons, data assimilation schemes that blend SST observations with ocean model dynamics have become well established (Bell *et al.*, 2000). In the case of short-range ocean forecasts, the initial surface boundary condition can be provided from timely remotely-sensed SST, which is kept constant throughout the forecasting period. However, the assumption that the observed SST field does not change significantly with time is not a reasonable one for medium- to long-range forecasts.

The potential of using microwave-derived SST data, with the provision of accurate, all-weather global coverage is being complimented by a wider research on its applicability. Apart from the orbiting TRMM satellite, the five-year old AMSR series of instruments onboard the AQUA and ADEOS-II satellites are now providing even more accurate retrievals of sea surface temperature data. This availability is leading to the generation of fused SST products as part of the GODAE High-Resolution SST Pilot Project (GHRSST-PP), consisting of twice-daily, global SST fields originally derived from the TMI and AMSR-E orbiting sensors (http://www.ghrsst-pp.org/).

The availability of these SST datasets can also address another prerequisite for the improvement of high resolution ocean models, i.e. objective forecast validation using appropriate, independent data. This issue already poses a difficulty for coarse resolution models, and the validation problem is far more significant to verify the skill of ocean models to forecast the seasonal high resolution variability because of the lack of appropriate spatio-temporal data.

The free surface, sigma coordinate Princeton Ocean Model (POM) is a well-established model that is being used for a variety of applications, ranging from small-scale process studies and coastal and estuarine modelling and prediction to basin-scale ocean circulation and climate change modelling (Ezer, 2000). In this study, POM is coupled to the atmosphere Eta model to forecast, at a high resolution, the ocean circulation over part of the Ionian basin (in Mediterranean Sea). The numerous air-sea processes that are active in this region provide a unique opportunity for observational and modelling studies (Robinson *et al.*, 2001).

This study attempts to improve the prediction of the POM model using data assimilation. Experiments are performed on a comparative basis, assimilating SST derived from (1) the Global Data Assimilation System (GDAS; Kanamitsu, 1989) modelled data and (2) the TMI-sensor. The resulting model output is compared with collocated observations. The scope of these experiments is to assess the effectiveness of assimilating passive microwave remotely-sensed data to improve high resolution ocean forecasting. These experiments also evaluate the benefit of optimising a Newtonian nudging scheme as an efficient data assimilation scheme for POM.

The other aim of this study is to derive suitable, region-specific AVHRR calibration algorithms and to apply exploratory spatial data analysis (ESDA) in order to analyse the spatial accuracy of the forecasted, high resolution ocean model fields.

2. Methodology

2.1. *Retrieval of Microwave-derived SST for model assimilation*

Each daily global coverage of the sea surface retrieved by the TMI is organised into seven ascending and descending datasets as follows: time of data retrieval, sea surface temperature, 10 m surface wind speed detected at 11 GHz, 10 m surface wind speed detected at 37 GHz, integrated precipitable water vapour, cloud liquid water, and precipitation rate.

Daily TMI data covering a full year period (January-December 1999) was retrieved by ftp from http://www.ssmi.com. The data is provided as binary data and cover a global region extending from 40^{o}S to 40^{o}N, and each daily data file consisted of fourteen 0.25^{o} x 0.25^{o} grid (1440, 320) byte maps. Two FORTRAN programmes were written to decode, process and interpolate the TMI data into Grid Analysis and Display System (GrADS)-format monthly set of sequential, daily ascending and descending data according to the grid resolution of the models. Since precipitation induces error in the retrieval of the geophysical parameters by the TMI sensor (Gentemann *et al*., 2004), rain pixels were used to mask off same-area pixels from the other collocated ascending and descending geophysical field maps. Valid geophysical data lay between 0 and 250 and pixels were scaled according to the calibration information supplied with the data as to obtain meaningful geophysical fields. TMI monthly datasets were displayed to note orbit time and the integrity of the SST and wind fields over the model domain area. This enabled the selection of the appropriate sets of SST data to initialise the Eta model at 00 UT and identification of co-temporal remotely-sensed geophysical fields to similar field elements predicted by the model. Special attention was given to the data used to initialize the model as to ensure insertion of good quality initial SST fields in the numerical model.

2.2. *Retrieval of infrared-derived SST*

The NOAA CoastWatch archive provided (1) raw 1.1 km AVHRR full channels data and (2) collocated NLSST data. This database was extensively used to derive an optimal calibration algorithm to be applied over the central Mediterranean. The following data were archived:

*Absorbing aerosols over the Atlantic Ocean***:** Daily data acquired by the Total Ozone Mapping Spectrometer (TOMS) satellite was retrieved by ftp from http://toms.gsfc.nasa.gov/ftpdata.html. The daily maps showed the absorbing aerosols over the Atlantic Ocean, which included the south and east coast of the United States. Days showing traces of absorbing aerosols were noted.

CoastWatch data: Data covering a period of two years (1998-1999) were retrieved from the NOAA CoastWatch Active Access System (http://coastwatch.noaa.gov/) for the South East Coast Node in the United States. This region has been selected in view of the full availability of data, including *in situ* buoy data (NODC) and GOES datasets. The area of interest extended from (32^{o}N, 73^{o}W) to (37^{o}N, 79^{o}W). The oceanic area was subdivided into sectors to facilitate data handling and processing (fig. 1).

Figure 1. The South East Coast was selected as one of the nodes of CoastWatch. The area was subdivided into sectors for the purpose of the present investigation.

An example of the extraction of AVHRR and related data (NLSST and collocated infrared radiances) from a sector that was free from aerosols and clouds (sector E) is shown in fig. 2. During the entire two-year period, a total of 286 sectors were extracted out of 31 AVHRR scenes were found to be aerosol- and cloud-free (table 1), from which channel 4 and 5 radiances and collocated NLSST values were extracted and archived.

Figure 2. Selection of valid channel 4 and 5 brightness temperatures (1.1 by 1.1 km pixel resolution) from individual sectors depended on the absence of clouds (using channel 1 CoastWatch data) and absorbing aerosols as detected by TOMS data.

Table 1. Cloud- and aerosol-free, valid geographical sectors (shaded in gray) from the South East coast area of the US. Visible and IR data from these sectors were retrieved during 1998 and 1999.

Derivation of multiple regression models based on the split window technique: The technique developed here is based on the relationship between the ratio of the variations of the satellite brightness temperatures derived from AVHRR channels 4 and 5.

For each collocated pixels relating to individual sectors, a table was produced listing the difference [TB_4-TB_5], the slope [$\Delta TB_4/\Delta TB_5$], and the collocated NLSST value for each set of collocated pixels. A potential contaminant was the unresolved cloud pixels in the analysis. Cloud detection in each valid sector was based on the amount of spectral information given for each pixel and on a combination of spectral channels (near-infrared and thermal infrared) as described by Kriebel (1996). These were (i) a simple ratio test was applied to filter out contaminated radiances as detected by channels 4 and 5, (ii) a gross cloud check, (iii) the Thin Cirrus Test and (iv) the Fog/Stratus Test were used.

Since the range of values for [TB_4-TB_5] and the slope [$\Delta TB_4/\Delta TB_5$] contain information about the instantaneous atmospheric water vapour profile, data rows having the same slope values were grouped together and archived. The pixel values for each slope [$\Delta TB_4/\Delta TB_5$] – specific group were merged together and a multiple regression model was derived.

To test the applicability of this approach over the central Mediterranean region, valid collocated brightness temperature data were calibrated and their profile in terms of [TB_4-TB_5] and [$\Delta TB_4/\Delta TB_5$] was extracted. According to the resulting profile extracted from this data, the appropriate SST multiple regression model was selected. These data were statistically compared with collocated TMI-derived SST scenes using basic statistical measures.

The accuracy of these models was compared against the linear mid-latitude algorithm derived by Coll *et al.*, (1994) for the Mediterranean using the French CMS-Lannion dataset. This dataset is composed of 348 points partly collected over the Mediterranean Sea (Antoine *et al.*, 1992). The optimised split-window algorithm (hereinafter referred to as Coll94) for this data is:

$$SST = TB_4 + 2.13(TB_4\text{-}TB_5) + 0.18$$

Calibration of high-resolution, infrared radiances acquired over the ocean model domain: Local Area Coverage (LAC) 1.1 km AVHRR imagery for the period July 20th 1999 to August 7th 1999 containing 16-bit, channels 3, 4 and 5 radiance data were retrieved from NOAA's Satellite Active Archive (http://www.class.noaa.gov). Raw infrared radiances from swaths covering the spatial domain of the ocean forecasting system (15.78^{o}E, 33.18^{o}N - 19.18^{o}E, 35.74^{o}N) were extracted and archived. To these raw images, panoramic distortion corrections, radiometric and sun angle corrections were applied. Scenes showing extensive contamination by cloud and dust were discarded. It proved very difficult to obtain valid AVHRR scenes over the area of interest during the 16-day time-frame, and only 5 suitable AVHRR overpasses were available (table 2). The remaining swaths where strongly affected by cloud cover and dust aerosols due to an episode of dust uptake from the Sahara desert that started on 22nd of July and reached the area of interest on the 26th of July 1999.

Suitable scenes were re-sampled to within the model domain to derive a new output consisting of separate channel 3, 4 and 5 radiances. Collocated pixels from each channels 4 and 5 were calibrated and their profile in terms of [TB_4-TB_5] and [$\Delta TB_4/\Delta TB_5$] was extracted. According to the resulting profile, the appropriate SST multiple regression model was selected. These data were statistically compared with TMI-derived SST scenes over the same model domain from their full-scene statistics (minimum, maximum, mean and standard deviation). The final 1.1 km by 1.1 km SST maps were used to validate, in spatial terms, the SST forecasts produced by the ocean model.

Table 2. Details of individual AVHRR LAC scenes, including data integrity, collected over the central Mediterranean during the period 20 July – 7 August 1999. (Source: Satellite Active Archive – NESDIS).

2.3. *Model description and configuration*

POM (Blumberg and Mellor, 1987) is a free-surface, three-dimensional finite-difference numerical model based on the primitive equations with Boussinesq and hydrostatic approximations. All the equations are written in rectangular coordinates and contain spatially and temporally varying horizontal eddy viscosity and diffusion coefficients. The model was implemented with a regularly spaced grid of 4 km in part of the Ionian basin. The model had 24 sigma coordinate levels that were distributed logarithmically in the bottom and surface boundary layers to increase resolution there. The model used the 2.5 Mellor–Yamada turbulence closure scheme (Blumberg and Mellor, 1987) and the Smagorinsky horizontal viscosity parameterization (Smagorinsky, 1963).

The ocean model integration domain (15.8^{o}-19.1^{o}E - 33.2 ^{o}-35.8^{o}N) consisted of 82 grid points in the east-west direction, and 61 grid points in the north-south direction, grid spacing of 0.042^{o} by 0.042^{o} latitude and longitude with 24 sigma levels in the vertical. The model followed a bottom-following sigma coordinate system. The number of vertical levels in the water column as the same everywhere in the domain irrespective of the depth of the water column, with 24 sigma levels in the vertical, which follow a logarithmic distribution near the surface in order to resolve the dynamics of the surface mixed layer. The basic equations follow the sigma coordinate system (Blumberg & Mellor, 1987). The basic equations (in horizontal Cartesian coordinates) are given in detail by Mellor (1998) in his *Users guide of the Princeton Ocean Model.*

In order to resolve the mixed layer better, the vertical resolution of the model was highest in the upper 100 m. The domain area covering the experimental oceanic area is characterised by a maximum depth of 4000 m. The re-interpolation of land/sea mask was based on the model grid points in the horizontal and vertical dimension was done from the GTOPO30 original file (http://edcdaac.usgs.gov/gtopo30/gtopo30.html). The entire integration domain covered the sea surface. The model bathymetry was re-interpolated to model grid points from a subset of the original US Navy Digital Bathymetric Base (with a nominal resolution of 0.083^{o} by 0.083^{o}) using bilinear interpolation.

The ocean model started with a hind-cast forecasting sequence on 1st July with zero velocity and continued for an additional 20 days. The model produced 3-D oceanic fields that were adjusted to a constant SST field derived from the TMI sensor on the 22nd of July 1999 at approximately 00 UT. The initial climatological fields were obtained using the Mediterranean Ocean Data Base (MODB-MED4). The lateral boundary conditions consisted of seasonal temperature, salinity, and ocean currents (u- and v-components) at standard depth levels as archived in the Mediterranean Ocean Data Base - MODB MED4 (http://modb.oce.ulg.ac.be/medmex/ss_st.html). The dataset consists of >34,000 hydrographic stations in the Mediterranean Sea taken from the U.S. National Oceanographic data Center (NODC) and the Bureau des Données Océaniques (BNDO) historical data banks (Brasseur *et al.*, 1996). For each season, initial fields at 36 depths levels were retrieved and read by the model and interpolated onto the 24-level σ-coordinate model sigma levels using the routine *ZTOSIG*. The MODB MED4 seasonal data sets with a horizontal resolution of 0.25^{o}.

2.4. *High resolution, predicted air-sea surface fluxes.*

The Eta atmosphere model was used to provide high-resolution spatio-temporal air-sea fluxes to initialize the ocean surface boundary conditions. This model is based on the National Centers for Environmental Prediction NCEP Eta regional atmospheric model (Mesinger *et al.*, 1988; Janjic, 1990, 1994). The Eta model dynamics uses numerical solutions controlled by conservation of integral properties, energetically consistent time-difference splitting, and the step-like

topography representation. The model physics include land surface processes, a surface layer scheme based on similarity theory, turbulent mixing, deep and shallow water convection, large-scale precipitation, lateral diffusion and radiation parameterization.

Figure 3 illustrates the integration domains of the regional and nested high resolution Eta model overlying the ocean model with the same grid size. Initial conditions for the regional model working at 0.17^o by 0.17^o horizontal domain, were obtained from the World Area Forecasting System and Global Data Assimilation System (GDAS; Kanamitsu, 1989). This model provided 36-hour forecasted boundary conditions to drive the nested high resolution model. The latter provided air temperature, dew point temperature at 2 m, surface turbulent and radiative heat flux forcings, total precipitation, surface pressure and wind stress as the forcing fields to the ocean model (fig. 4).

Figure 3. Domains of the limited area, Mediterranean-wide Eta model (LAT: 29.00^o – 47.50^oN; LON: -10.00^oW – 42.00^oE). Nested within its integration domain is the high-resolution Eta model (LAT: 33.24^o – 35.74^oN; LON: 15.74^o – 19.17^oE).

Figure 4. Input of 3-hourly forecasts of atmospheric air-sea flux fields into POM as its initial surface boundary conditions.

2.5. *Model integration*

The pre-processing phase consisted of defining the model domain, preparation of lateral and surface boundary conditions, data decoding, formatting and data interpolation.

The ocean model was allowed to perform a hind-cast run for the first 21 days of July to produce 3-D oceanic fields that were adjusted to a constant SST field derived from the TMI sensor on the 22nd of July 1999 at approximately 00 UT to nudge the fields as much as possible to the oceanic-state of the 22nd July 1999.

The ocean model was forced at each grid point by same-day, 3-hourly forecasted air-sea fluxes at exactly the same horizontal resolution. This daily forcing mode started on the 22 July and lasted until 6 August 1999. The atmosphere model provided air temperature, dew point temperature at 2 m, sea level atmospheric pressure, surface turbulent and radiative heat flux forcings, total precipitation, surface pressure and wind stress.

2.6. *The assimilation scheme*

The data assimilation mode consisted of a pre-forecast model run that adjusted the model fields towards the interpolated TMI-derived SST by nudging the initial values at all data points towards the observed data. The blending estimate was a scalar linear combination, with an assigned weight, of the modelled and data values at all grid points. The nudging coefficient was related to dynamical scales and *a priori* estimates of model and data errors used to assimilate SST into the ocean model. The pre-forecast run used the initial, 3-hourly ocean fields previously forecasted by the ocean model. The model fields were then "relaxed" towards the SST target field by using the prognostic equation with the correction term of the form:

$$\frac{\partial q^{\text{model}}}{\partial t} + A_q + K_q(q_n^{\text{model}} - q_n^{\text{observations}}) = 0$$

where q^{model} is the model variable; $q^{\text{observation}}$ is the target analysis; A_q is one of the model terms in the dynamical equations such as advection and diffusion and K_q is the relaxation coefficient. The time level *t*, is the value at which model predictions and observation are made. The equation represents the difference between the model solution and the corresponding observation. The subscript *n* indicates the time level at which model predictions and observations are made. The tendency of the model prognostic variable $\partial q^{\text{model}}$ provides the q_n^{model} at the next time level (n+1). The equation is modified by introducing the relaxation term K_q $(q^{\text{model}} - q^{\text{observation}})$ that nudges the predicted variable q^{model} to the observed value on the relaxation time scale. K_q, the

relaxation function (in x,y,z,t), which in this study is kept constant throughout the pre-forecast run. The role of transferring the assimilated information in the vertical and horizontal is performed by the model itself in a pre-forecast run, acting as a dynamical interpolator/extrapolator.

In the forecasting mode, the model used the adjusted model fields represented at each model grid points to initialize its boundary conditions every three hours.

2.7. *Fine-tuning of the data assimilation scheme.*

In order to identify the best nudging conditions for the ocean model, a data assimilation (DA) experiment was performed to assess the effectiveness of (i) varying the nudging period and (ii) including a nudging coefficient, to force the model fields towards the SST observations. Four nudging coefficients were tested $5x10^{-3}$, $5x10^{-4}$, $5x10^{-5}$ and $5x10^{-6}$ for each of three nudging periods. The coefficient values were selected on the basis of an empirical value previously selected for data assimilation purposes by POM (Blumberg and Mellor, 1987). A separate control run was performed without a data assimilation scheme.

2.8. *Validation of the assimilation system*

The post-processing stage generated the predicted oceanic fields in gridded xyz variables for subsequent standard and diagnostic model verification against same-area , 1.1 km pixel resolution SST observations.

The forecasting performance of the ocean model was analysed using basic statistical performance measures such as mean, standard deviation, bias and Root Mean Square Error.

Surface analysis was performed to outline and compare forecasted fields with high-resolution information of the ocean surface derived by remote sensing.

3. Results and discussion.

3.1. *Linear regression modelling using the split-window technique*

The split-window technique is the most useful atmospheric correction method for SST derived by infrared sensors (Arbelo *et al.*, 2000). One of the usual approaches to calibrate AVHRR scenes is to perform regression analysis between IR channels centered at 11 and 12 μm and the atmospheric profiles generated by a radiative transfer model. The coefficient of the SST algorithm can then be determined synthetically. An alternative approach can be taken by using, instead of a model, the differential absorption of the two split-window channels 4 and 5 due to water vapour (Mathew *et al.*, 2001). In this case, the corresponding difference in brightness temperature will give a signature of the atmospheric water vapour profile. With the availability of calibrated temperature brightness from channels 4 and 5 and collocated SST estimation that were derived from the CoastWatch database, the coefficients were derived empirically at the pixel level. This approach offered the advantage of deriving more accurate regression models based on region-specific atmospheric profiles. In so doing, this study attempted to derive a range of split-window coefficients each reflecting particular vertical atmospheric water vapour profiles as defined by the slope $[TB_4/TB_5]$, ranging from 1.01 to 0.86.

The equations presented in table 3a-b are the linear equation models derived from the multiple regression between NLSST, TB_4, and the difference between TB_4 and TB_5. The dependent variable (NLSST) is linearly correlated to the independent ones (TB_4 and TB_4-TB_5) throughout the analysis, with strong R^2 and mostly similar partial regression coefficients for each of the independent variables over the entire range of slope $[\Delta TB_4/\Delta TB_5]$ values. In his review on SST algorithms retrieved by infrared sensors, Barton (1995) referred to the same split window formalism where the partial regression coefficient related to TB_4 is close to unity. As is the case in table 3a-b, this value of coefficient implies that at the lowest order, the sea surface temperature equals the measured brightness temperature. The other coefficient related to the differential absorption between channels 4 and 5 (or the slope $[\Delta TB_4/\Delta TB_5]$) is equivalent to the transmittance through the atmosphere from the surface to the satellite and is dependent on both the mass

absorption coefficient of the atmospheric absorbers and the path length (Barton, 1995). The dependence of this coefficient on the temporal structure of the atmospheric vertical profile always induces a degree of variability, as shown by the present results.

Table 3a. Table containing the suite of single line equations valid for different atmospheric states as defined by their slopes ranging from 1.01 to 0.94. The regression analysis was done over a two-year period over the CoastWatch area. Regression models are statistically significant at the 1% level (P-value <0.01).

Table 3b. Table containing the suite of single line equations valid for different atmospheric states as defined by their slopes ranging from 0.93 to 0.86. The regression analysis was done over a two-year period over the CoastWatch area. Regression models are statistically significant at the 1% level (P-value <0.01).

Coll *et al.* (1994) associated the constant (i.e. - intercept) of the split window algorithm to the emissivity effect and Barton (1995) showed that it can range from 28 to –17 for a total of 21 algorithms used to retrieve SST through subtropical atmospheres. This is also the case for the resulting regression models, where each equation refers to particular atmospheric vertical profiles as detected by the two infrared channels.

Tables 3a-b also provide an indication of the magnitude of the residuals for each group of slopes (mean absolute residual error and number of Studentized residuals). Further analysis of these residuals may stabilise even further the regression models. The presence of undetected, contaminated pixels, as well as the inherent inaccuracies of the dependent variable (NLSST), may have given rise to some instability. Uncertainties do however exist in these measurements, which include the accuracy of the original NLSST dataset, the contamination of unresolved cloud and aerosols and errors in the satellite calibration.

The dependency and sensitivity of $[\Delta TB_4/\Delta TB_5]$ on the atmospheric transmittance shows that it is not proper to use globally-retrieved coefficients from NESDIS to correct regional SST imagery with enough accuracy. This was also expressed by Sobrino *et al.* (1993) after they observed the impact of the atmospheric transmittance and total water vapour content on SST retrieval from AVHRR.

Although the approach used is similar in concept to that developed by Sobrino *et al.* (1993), it is technically different and simpler. In their work, they have simulated channels 4 and 5 of AVHRR/2 of NOAA-11 using a radiative transfer model with a range of atmospheric conditions and surface temperature that reflected a worldwide variability. The present study uses instead the empirical knowledge derived from the NOAA AVHRR readings from channels 4 and 5 and collocated NLSST pixels to derive the algorithms. Indeed, the slope $\Delta TB_4/\Delta TB_5$ was calculated for each collocated pair of pixels (a total of 203,010 pixels) and the resulting mean slope for each sector was categorised to represent the water vapour profile of different atmospheric states during a 2-year period. This grouping was necessary to average out the errors inherent in this method, which may originate from the inaccuracy of the original NLSST dataset embedded in any split-window algorithm (an average of ± 0.14 ^{o}C against *in situ* data – [Li *et al.*, 2001]), the contamination of unresolved cloud and aerosols, and errors in the sensor calibration. Similar errors are also encountered when such line algorithms are derived by regressing brightness temperature from channels 4 and 5 against *in situ*, collocated data.

It is interesting to note that the trend of the TMI-derived integrated precipitable water vapour over the area of interest during the period of 20th July to 7th August 1999 (fig. 5) increased from 2.2 to around 3.0 g cm^{-2}. This profile cannot be considered as homogeneous over the area of interest and is attributed to the particular climatological conditions over the central Mediterranean

Figure 5. TMI-derived daily integrated precipitable water vapour (g cm^{-2}) over the area of interest during the period 20 July to 7 August 1999.

3.2. *Calibration of AVHRR scenes over the Ionian basin*.

The performance of these regression models for the Mediterranean region was assessed for suitable NOAA AVHRR images acquired between 20th July and 7th August 1999 over the Ionian basin (table 2). Lermusiaux and Robinson (2001) encountered a similar lack of suitable data trying to verify their 16-day model integration run, for which only four AVHRR scenes were found to be suitable for comparison. Table 4 gives a summary of the performance of the regression model approach for the valid AVHRR scenes.

Table 4. Performance of linear regression models for valid AVHRR scenes over the area of interest against microwave-derived SST and the mid-latitude algorithm derived by Coll *et al.*, (1994). Inter-comparison was done on the basis of entire scene statistics.

Since no collocated set of *in situ* match-up data was available from the study area, the accuracy assessment of the regression models was based on an independent set of collocated SST derived from the TMI sensor. The assessment was based on the average difference of collocated [$SST_{algorihtm}$ minus SST_{TMI}]. Sobrino *et al.*, (1993) used a similar approach to assess the accuracy of their results by comparing their algorithms to an independent set of CPSST and MCSST data.

Despite the lack of *in situ* data, and the use of a small number of suitable AVHRR imagery, this study provided some interesting results. Generally, the regression modelling gave a very close estimate of SST that was consistent with the SST_{TMI}, but at a much finer resolution, with the regression modelling approach offering a wide range of possible single-line equations depending on particular atmospheric conditions. A degree of inherent difference between the two datasets is always expected due to the fact that the accuracy of the regression models is based on the bulk SST sampled by buoys (in the case of NLSST), while the TMI-retreived SST is the 1 mm thick *sub-skin* SST.

Results indicated that for the selected AVHRR imagery, appropriate selection and use of the regression models fared better than the Coll94 algorithm. The use of both algorithms is encouraging, with the regression modelling approach offering a wider range of possible single-line equations depending on particular atmospheric conditions, whereas the regional one (i.e. Coll94) is not flexible at all. Antoine *et al.*, (1992) gave an error estimate of 0.75 K for the Coll94 algorithm, which can be improved by taking into account scan angle effects. The Coll94 and the regression modelling approach display similar amount of small standard deviation, indicating a certain degree of robustness. This similarity gives some confidence in using the linear regression approach for the calibration of AVHRR imagery.

There is still considerable room for improvement of this approach. To do this, multi-year AVHRR passes over the area of interest need to be calculated, calibrated and compared with independent data.

3.3. *Effectiveness of data assimilation on the forecasting quality of the ocean model*.

No data assimilation scheme

Figure 6 shows the results when the SST assimilation scheme was inactive. The increased RMSE index was based on the comparison between the forecasted SST field and collocated SST derived by the passive microwave sensor. An increased standard error with time was also shown by the bias index, giving a maximum under-forecasted SST value of more than 2°C at the end of the full

model integration run. The results showed the importance of data assimilation, the absence of which leads to a significant model error drift and propagation of misfits in the forecasted SST.

Figure 6. Bias trend between 24-hr predicted SST and collocated observed SST throughout the 15-day model integration of POM with no data assimilation scheme.

Newtonian relaxation towards SST with variable nudging periods and coefficients.

Results are presented in fig. 7a-d in the form of linear trends of the resulting biases between the 24-hr forecasted SST fields against collocated observations. Despite the small period of evaluation, some general remarks can be made. The overall result showed that a longer nudging period always resulted in a better prediction of the SST field, and a best combination of the values for the coefficient and nudging period occurs when they are set at 5 x 10^{-4} and 12 hrs respectively. This combination gave an average bias of -0.07 ^{o}C. Not so accurate forecasts were achieved with increasing nudging values, reaching a maximum bias of greater than 1^{o}C when the coefficients are not strong enough to nudge the model fields towards the observations.

Figure 7a-d. Bias trend between the SST forecasts produced by the ocean model with using a nudging coefficient of (a) 5x10^{-3} (b) 5x10^{-4} (c) 5x10^{-5} and (d) 5x10^{-6} with different nudging periods.

These settings lead to an overall improvement in the performance of the ocean model, leading to one of the best SST forecasts ever achieved in the region. Nittis *et al.*, (2001) for example, for example, obtained a bias of 0.1 to 0.8 ^{o}C when their 24-hour POM-forecasted SST was compared to collocated in situ buoy measurements.

One drawback in the present study is the short initialisation time of the ocean model that starts with zero velocity. Ideally, POM should start a couple of thousand years before the actual experiment to allow the model to reach a well-maintained statistically steady thermohaline and equilibrated system at all model levels in the water column, along with budgets of heat and freshwater and their seasonal variabilities (Wu and Hains, 1996).

3.4. *Spatial analysis of the forecasted fields*

The validation of the high-resolution forecasts required the availability of comparable observations that captured the small-scale variability of the ocean-state during the integration period of the ocean model. An example of some of the datasets used to initialise, assimilate and verify the predicted oceanic fields is given in figure 8a-d. Starting with the calibrated AVHRR data, scenes retrieved on the 22nd and 23rd July 1999 show very interesting thermal patterns. These very high-resolution datasets were an optimal source for *comparative* analysis of the spatial accuracy of the forecasted SST fields (~ 4 km grid spacing).

Figure 8 a-d. An overview of some datasets used to initialise, nudge, and verify the predicted oceanic fields. The thermal profiles (a) and (c) were retrieved by the NOAA AVHRR sensor on the 22nd and 23rd July 1999. The thermal profiles (b) and (d) were retrieved by the passive microwave TMI sensor. In spite of the coarser detail identified by the TMI sensor, the thermal signature is still evident (aided by contours), including major filaments originating from the cold core.

The SST derived from the NOAA AVHRR infrared sensor during these two days revealed a surface variability that can be associated with major oceanic currents in the Ionian basin. Associated with these ocean fronts were features such as filaments and jets with scales of tens of km down to 5 km similar to the ones described by Gascard (1978). Figure 8a shows a calibrated image retrieved by the NOAA AVHRR sensor on the 22nd of July 1999, exhibiting an interesting thermal feature that was evolving in the area of interest. This feature forms part of the transient but recurrent gyre described by Robinson and Golnaraghi (1994), having considerable fine detail of the intense curling and filamentous jets extruding from the main path of the cold water inflow that is migrating to the north-western part of the integration domain.

Figure 8b shows an SST map derived by the lower-resolution TMI sensor some ten hours earlier than the same-day AVHRR image (fig. 8a). In spite of its coarser detail, the thermal signature was still evident, including major filaments originating from the cold core. Recognition of the main thermal feature is aided by contour lines to delineate the major gradients of the SST profile. The spatial offset of the surface feature is probably explained by the 11-hour difference between the TMI and AVHRR swaths.

Similarly, figures 8c and d compliment each other both quantitatively and qualitatively. The eddy's slight decrease in intensity from the 22nd to the 23rd of July was also detectable by the TMI sensor. Figure 8a-d suggests that this gyre was evolving and moving north-westerly.

A dust plume was observed to evolve over the model integration period during 23 July 1999 originating from the Libyan-Tunisian region in North Africa. Independent forecasts of this dust plume showed that the amount of dust load increased and affected the entire area of interest. This corresponded with the lack of suitable AVHRR scenes from the 24 July until 7 August 1999.

The modelled data generated by this study show a balance of atmospheric (provided by the high resolution, nested Eta model) and oceanic dynamic processes (provided by the high resolution POM), including atmospheric heating and cooling and wind momentum (fig. 9 a-d), and horizontal advection in the ocean (fig. 10). The connection between the predicted 10 m wind magnitude on the 23rd of July and the surface temperature field are somewhat striking. Because of their duration, strength and orientation, the corresponding winds have a tendency to strengthen both the structure and migration of the thermal feature identified in figure 8. A closer inspection of figure 11 shows the occurrence of stronger ocean currents along the SST gradients.

Figure 9 a-d. Predicted and observed fields on 23.07.99 at 00:00 UT. The sensible heat flux (a) corresponds to the predicted 2 m air temperature (b), and the predicted (c) and observed (d) 10 m wind magnitude (m s^{-1}).

Figure 10. 12-hour forecast of the sea surface elevation (m) predicted by the ocean model (using DA scheme 1; τ=24 hours) starting at 22.07.99 00 UT. The surface flow is characterised by a slightly elevated sea surface.

Figure 11. Direction and magnitude (cm s^{-1}) of the surface ocean currents as predicted at the 36th hour from the start of the model integration on the 22nd of August 1999 at 00 UT. TMI-SST was assimilated using scheme 1 with a τ = 24 hrs. (Scale arrow is 0.4 cm s^{-1}).

The close similarity between the SST maps derived from the two orbiting sensors demonstrate the potential of using the all-weather TMI-derived SST to initialise the boundary conditions of the ocean model and to dynamically adjust the model fields. The continuous availability of TMI-retrieved SST during the model integration period also facilitated the analysis of the forecasting skill of the ocean model to forecast SST fields in the absence of *in situ* data from the area of interest.

Figures 12 a - c illustrate the observed and predicted SST fields within a subset of the area of interest following the initialisation of the ocean model on the 22nd July. The 24-hour forecasted SST field, which is equivalent to 23rd July at 1200 UT is shown (fig. 12c). Main features can be noticed that are complimentary to the thermal pattern defined by the microwave SST retrieved on 23rd (fig. 8d) and 24th of July (fig. 12b) but with a higher structural definition than the TMI SST fields. This high definition closely matches the AVHRR image shown in figure 12a. Features such as the cool vortex A, the cool filament at B, the warmer pool C and the sharp temperature gradient at E, were easily traceable. Model data indicated that the direction and magnitude of the predicted ocean surface currents (fig. 11) were strongly linked to the gradients present in this vortex. The highly resolved, surface currents predicted by the ocean model gave further support to the ability of the ocean model to resolve oceanic circulation at a very high resolution. The formation and propagation of a colder area as predicted by the ocean model (lower left portion fig. 12b) agrees with the observed SST acquired by the TMI sensor acquired 12 hours later (fig. 12c).

Figure 12 a-c. SST features as (a) retrieved by AVHRR on the 23rd July 1999 at 12:41 UT , (b) predicted SST field for 23rd July 1999 at 12:00 UT (using DA scheme 1; τ=24 hours), and (c) as retrieved by TMI sensor on the 24th July 1999 at approximately 00:00 UT.
A=cool vortex; B=cool filament; C=warmer pool; D & E= temperature gradients.

3.5. *Spatial analysis of the final forecasted SST field.*

This part focused on the spatial accuracy of the surface temperature fields predicted at the end of the 15-day forecast run. This analysis was based on SST observations available from passive microwave remote sensing and re-interpolated to the same high-resolution model grid. No profiles were studied in the vertical dimension since no profile data was available. The availability of vertical profiles of temperature and salinity would have assisted the analysis of the error projection in the vertical dimension. It would also have been useful to assess how the data assimilation affects the dynamics of the underlying variables, with a resultant effect on the surface temperature.

Figure 13a represents the final SST field used to nudge the model fields starting on 05.08.99 at 1200 UT. This field was retrieved on 04.08.99 at 21.7 UT by the TMI sensor. Figure 13b is the 00 UT predicted SST field. To better resolve the predicted spatial structure, a 5x5 edge preserving smoothing kernel plus an additional low-pass 5x5 kernel were used to enhance the forecasted thermal pattern. Figure 13c represents the SST retrieved by the TMI sensor on 06.08.99 at 2100 UT. A cold tongue is evident, which was also seen in the forecasted field, but which was seen to be located further south. This offset was due to a 3-hour difference between the forecasted and remotely sensed field.

Figure 13 a-c. Model predicted SST on 6th August at 00 UT using the optimal settings identified for the data assimilation using TMI-derived SST and the set of air-sea fluxes predicted by the atmosphere model to drive the underlying ocean model.

It should be noted that the initial remotely-sensed SST fields used for assimilation throughout the entire 15-day period had an orbital time of ± 3 hours close to 00 UT. Errors arising from this gap in co-temporality with the initialisation time at 12 UT need therefore be taken into account. This also stands for the validation of the model predicted SST fields, which were out of phase with the TMI data by a maximum of ± 3 hours. No additional, collocated SST observations were available and therefore this error cannot be quantified. Henceforth, the present performance measures are based on a general, relative bias and RMSE rather than on the absolute value of the forecasts. Similar problems in data assimilation and model verification are always expressed, such

as the case of Gavart *et al.*, (1999) using TOPEX/POSEIDON data assimilation for ocean modelling and verification purposes.

Another limitation of this study was the short, 15-day model integration period. This limit was defined by the availability of integral TMI orbital swaths over the area of interest, which was needed to continuously initialise the surface boundary conditions of the POM model. It is interesting to note that similar, short-scale studies are not uncommon in the case of ocean modelling studies. Onken *et al.*, (2003) for example, studied the synoptic circulation and transport in the Tunisia-Sardinia-Sicily region using a model initialisation period of 12 days.

The creators of POM attempted to measure the benefits of assimilating AVHRR-SST into POM (Ezer and Mellor, 1997), but unlike the present study, their validation method was based simply on the visual observation of the predicted Gulf Stream against observations. The authors recommend the combined use of sea surface temperature and sea surface height (obtained by orbiting altimeters) to improve the model skill at lower depths.

4. Conclusion

In this study the data derived by the orbiting microwave sensor onboard the TRMM satellite was central to (1) provide initial SST data for the ocean model, and (2) model verification. The optimal adjustment of the data assimilation scheme to assimilate SST for the POM model to adjust the model fields towards the remote sensing observations was central.

The sub-mesoscale spatial information provided by the remotely-sensed, high-resolution thermal ocean maps was well-simulated as a result of the efficient data assimilation scheme identified by this study. The predicted information on the surface water circulation produced by this study was much more detailed than the latest investigations using POM over the same study area for a ten-day ocean simulation (Horton *et al.*, 1997).

The AVHRR calibration approach presented by this study is a powerful modelling tool that is able to provide appropriate split-window coefficients that best match the atmospheric composition detected by individual AVHRR scenes acquired over any geographical area. In this manner a suite of single line equations suitable for different atmospheric states have been produced as recommended by Steyn-Ross *et al.*, (1999). The modelling of the atmospheric composition using 31 AVHRR scenes collected over a two-year period provided a statistically robust approach to calibrate AVHRR scenes over a range of atmospheric profiles without the need of collocated *in situ* SST data. These single-line equations can be further fine-tuned and be made area-specific by augmenting them with new split-window data extracted from AVHRR scenes collected from specific geographical regions over the entire range of atmospheric variability. In this manner, a finer range of slope variation based on a high statistical significance can be defined from the relevant imagery.

The future of microwave-derived SST, with its provision of accurate, all-weather global coverage will be soon be complimented by an even wider research on its applicability. This study can be viewed as one of the first attempts to utilise this data source to improve the predictive capability of ocean forecasting systems. Apart from the orbiting TRMM satellite, the operational AMSR series of instruments on AQUA and ADEOS-II are now providing even more accurate retrievals of sea surface temperature data. This availability is leading to the generation of fused SST products requiring various strategies addressing the issues of retrieval and inter-calibration, scale, timing and location of observation, data interpolation and fusion (GHRSST-PP Science Team, 2005).

Acknowledgements

This work was carried using the computing facilitates of the Euro-Mediterranean Centre on Insular Coastal Dynamics (Council of Europe, Malta). The technical support and guidance of Svetlana Music, Slobodan. Nickovic, Bosko Telenta, and Goran Pejanovic is much appreciated. The support of the Director of the Centre, Anton Micallef, is duly acknowledged. The authors are

also grateful to Remote Sensing Systems (www.remss.com), sponsored by the NASA Earth Science REASoN DISCOVER Project, for making available important data used in this work.

References

Antoine, J.Y., Derrien, M., Harang, L., Borgne, P., Le Gleau, H. and Le Goas, C., (1992), Errors at large satellite zenith angles on AVHRR derived sea surface temperatures. International. Journal of Remote Sensing, 13, 1797-1804.

Arbelo, M., and Herrera, F., (1995), Comparison of total water vapour content obtained from TOVS-NOAA with radiosoundings data in Canary Islands zone. Atmospheric Sensing and Modelling II (Santer R.P., ed.)., SPIE Proceedings Vol. 2582, pp 178-184, ISBN: 0-8194-1946-X.

Barton I.J., (1995), Satellite-derived sea surface temperatures: Current status. Journal of Geophysical Research, 100, C5, 8777-8790.

Bell M.J., Forbes R.M., and Hines A., (2000), Assessment of a Global Data Assimilation System for real-time operational ocean forecasting. Journal of Marine Systems, 25, 1-22.

Blumberg A.F., and Mellor G.L., (1987), A description of a three-dimensional coastal ocean circulation model, Heaps N.H., (ed.), Three-dimensional coastal ocean circulation models. Coastal Estuarine Science., Vol. 4, pp 1-16, AGU, Washington, DC.

Brasseur P., Beckers J.M., Brankart J.M., and Schoenauen R., (1996), Seasonal temperature and salinity fields in the Mediterranean Sea: Climatological analysis of a historical data set. Deep Sea Research, Part II, 43, 2, 159-192.

Chassignet E. P., Bell M. J., Brasseur P., Evensen G., Griffies M., Hurlburt H. E., Leprovost C., Madec G., McClean J., Verrron J., Wallcraft A. J., (2004), The Modeling Component of Ocean Forecasting. The Global Ocean Data Assimilation Experiment Second Symposium 1-3 November, St Petersburg FL, USA

Coll C., Caselles V., Sobrino J.A., and Valor E., (1994), On the atmospheric dependence of the split-window equation for land surface temperature. International Journal on Remote Sensing, 15, 105-122.

Day C., (2000), Two satellites observe details of ocean-atmosphere coupling. Physics Today, June 2000, 23-24.

Ezer T., (2000), On the seasonal mixed-layer simulated by a basin-scale ocean model and the Mellor-Yamada turbulence scheme. Journal of Geophysical Research, 105, C7, 16843-16855.

Ezer T., and Mellor G.L., (1997) Data assimilation experiments in the Gulf stream region: How useful are satellite-derived data for nowcasting the subsurface fields? Journal of Atmospheric and Oceanic Technology, 14, 1379-1391.

Gascard, J.-C., (1978), Mediterranean deep water formation baroclinic instability and oceanic eddies. Oceanologica Acta, 1, 3, 315-330.

Gavart M., De Mey P., and Caniaux G., (1999), Assimilation of satellite altimeter data in a primitive-equation model of the Azores-Madeira region. Dynamics of the Atmosphere and Oceans, 29, 217-254.

Gentemann C.L., Wentz F.J., Mears C.A., and Smith D.K., (2004), *In situ* validation of Tropical Rainfall Measuring Mission microwave sea surface temperatures. Journal of Geophysical Research, 109, C04021.

GHRSST-PP (2005) report of the 6th GODAE High resolution SST Pilot Project Science Team Meeting, Met Office, Exeter, United Kingdom, May 14th-20th 2005. GHRSST-PP Report: GHRSST/21, 2005, 222pp

Hoke J.E., and Anthes R.A., (1976), The initialisation of numerical models by a dynamic initialisation technique. Monthly Weather Review, 104, 1551-1556.

Horton C., Clifford M., Schmitz J., and Kantha L.H., (1997), A real time oceanographic nowcast/forecast system for the Mediterranean Sea. Journal of Geophysical Research, 102, 123-125.

Janjic Z.I., (1990), The step-mountain coordinate: physical package. Monthly Weather Review, 118, 1429-1443.

Janjic Z.I., (1994), The step-mountain Eta coordinate model: further developments of the convection, viscous sublayer and turbulence closure schemes. Monthly Weather Review, 122, 927-945

Kanamitsu M., (1989), Description of the NMC Global Data Assimilation and Forecast System. Weather and Forecasting, 4, 3, 335-342.

Kriebel K.T., (1996), Cloud detection using AVHRR data. Advances in the use of NOAA AVHRR Data for land application (G. D'Souza *et al.*, eds.), ECS, EEC, EAEC, Brussels and Luxembourg, 195-210.

Lermusiaux P.F.J., and Robinson A.R., (2001), Features of dominant mesoscale variability, circulation patterns and dynamics in the Strait of Sicily. Deep-Sea Research, I, 48, 1953-1997.

Li X., Pichel W., Maturi E., Clemente-Colon P., and Sapper J., (2001), Deriving the operational non-linear multichannel sea surface temperature algorithm coefficients for NOAA-15 AVHRR/3. International Journal of Remote Sensing, 22, 4, 699-704.

Kanamitsu M., (1989), Description of the NMC Global Data Assimilation and Forecast System. Weather and Forecasting, 4, 3, 335-342.

Mathew K., Nagarani C.M., and Kirankumar A.S., (2001), Split-window and multi-angle methods of sea surface temperature determination: an analysis. International Journal of Remote Sensing, 22, 16, 3237-3251.

Mellor G.L., (1998), Users guide for a three-dimensional primitive equation, numerical ocean model. Progress in Atmospheric and Oceanic Science, Princeton University, 41 pp. Available at <http://www.aos.princeton.edu/WWWPUBLIC/htdocs.pom/>.

Mesinger F., Janjic Z.I., Nickovic S., Gavrilov D., and Deaven D.G., (1988), The step-mountain coordinate: model description and performance for cases of Alpine lee cyclogenesis and for a case of an Applachian redevelopment. Monthly Weather Review, 116, 1493-1518.

Nittis K., Zervakis V., Perivoliotis L., Papadopolous A., and Chronis G., (2001), Operational monitoring and forecasting in the Aegean Sea: System limitations and forecasting skill evaluation. Marine Pollution Bulletin, 43, 7-12 154-163.

Onken R., Robinson A.R., Lermusiaux P.F.J., Haley P.J., and Anderson L.A., (2003), Data-driven simulations of synoptic circulation and transports in the Tunisia-Sardinia-Sicily region. Journal of Geophysical Research, 108, C9, 8123-8136.

Robinson A.R., and Golnaraghi M., (1994), Physical and dynamical oceanography of the Mediterranean Sea. Ocean Processes in Climate Dynamics: Global and Mediterranean examples (Malanotte-Rizzoli P., and Robinson A.R., eds.), 255-306, Kluwer Academic Publishers.

Robinson A.R., and Lermusiaux P.F.J., (2001), Data Assimilation in Models. Encyclopedia of Ocean Sciences, Academic Press Ltd., London, 623-634.

Robinson, A.R., Theocharis A., Lascaratos A., and Leslie W.G., (2001), Mediterranean Sea Circulation. Encyclopedia of Ocean Sciences, 1689-1706, Academic Press Ltd., London.

Smagorinsky J., (1963), General circulation experiments with the primitive equations, I: The basic experiment. Monthly Weather Review, 91, 99-164.

Steyn-Ross M.L., Steyn-Ross D.A., and Jelenak A., (1999), Comparison of atmospheric correction algorithms for deriving sea surface temperature from AVHRR. International Journal of Remote Sensing, 20, 18, 3515-3531.

Sobrino J.A., Li L.Z., and Stoll M.P., (1993), Impact of the atmospheric transmittance and total water vapour content in the algorithms for estimating sea surface temperature. IEEE Transactions on Geoscience and Remote Sensing, 31, 5, 946-952.

Wu P., and Haines K., (1996), Modeling the dispersal of Levantine Intermediate Waterand its role in the Mediterranean deep water formation. Journal of Geophysical Research, 101, 3261–3271.

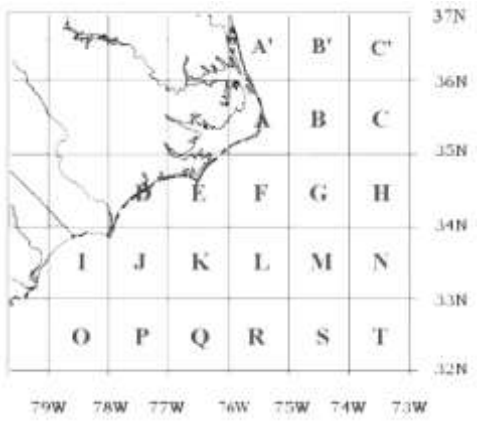

Figure 1. The South East Coast was selected as one of the nodes of CoastWatch. The area was subdivided into sectors for the purpose of the present investigation.

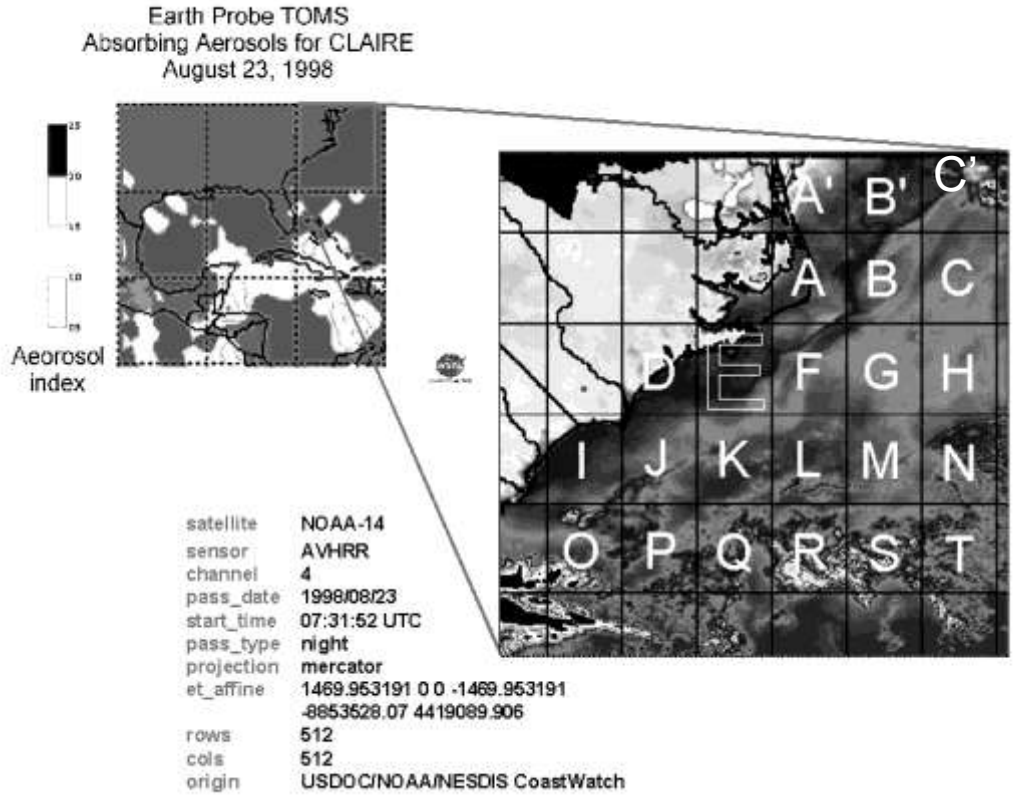

Figure 2. Selection of valid channel 4 and 5 brightness temperatures (1.1 by 1.1 km pixel resolution) from individual sectors depended on the absence of clouds (using channel 1 CoastWatch data) and absorbing aerosols as detected by TOMS data.

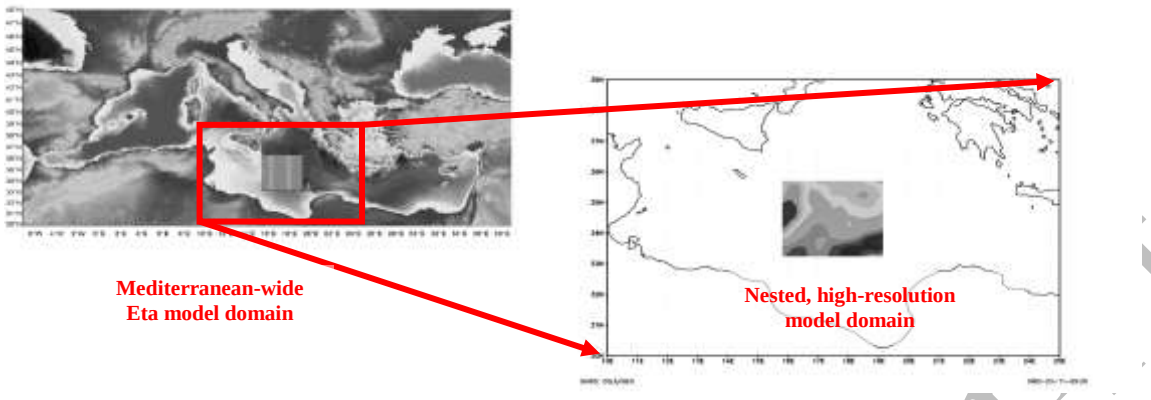

Figure 3. Domains of the limited area, Mediterranean-wide Eta model (LAT: 29.00^o – 47.50^{o}N; LON: -10.00^{o}W – 42.00^{o}E). Nested within its integration domain is the high-resolution Eta model (LAT: 33.24^o – 35.74^{o}N; LON: 15.74^o – 19.17^{o}E).

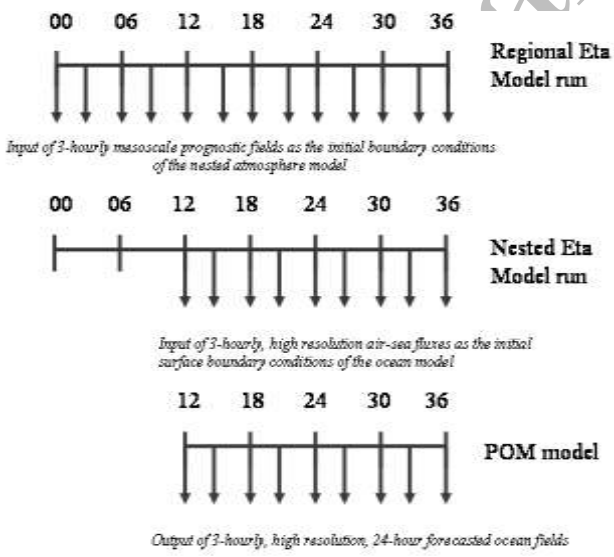

Figure 4. Input of 3-hourly forecasts of atmospheric air-sea flux fields into POM as its initial surface boundary conditions.

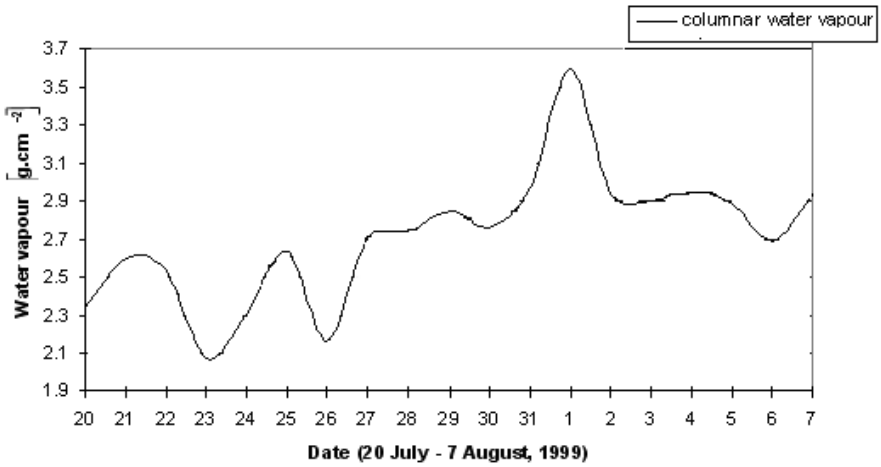

Figure 5. TMI-derived daily integrated precipitable water vapour (g cm^{-2}) over the area of interest during the period 20 July to 7 August 1999.

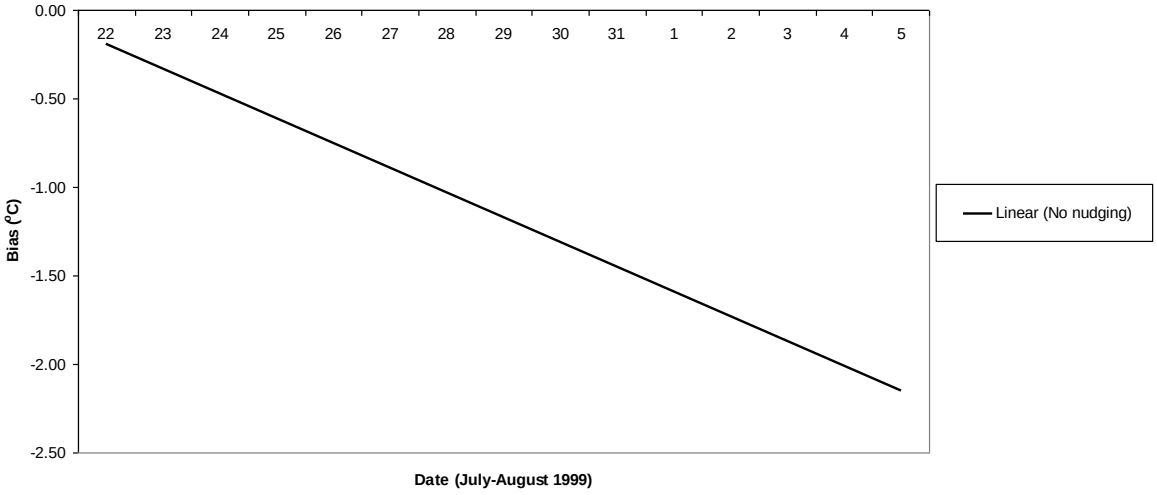

Figure 6. Bias trend between 24-hr predicted SST and collocated observed SST throughout the 15-day model integration of POM with no data assimilation scheme.

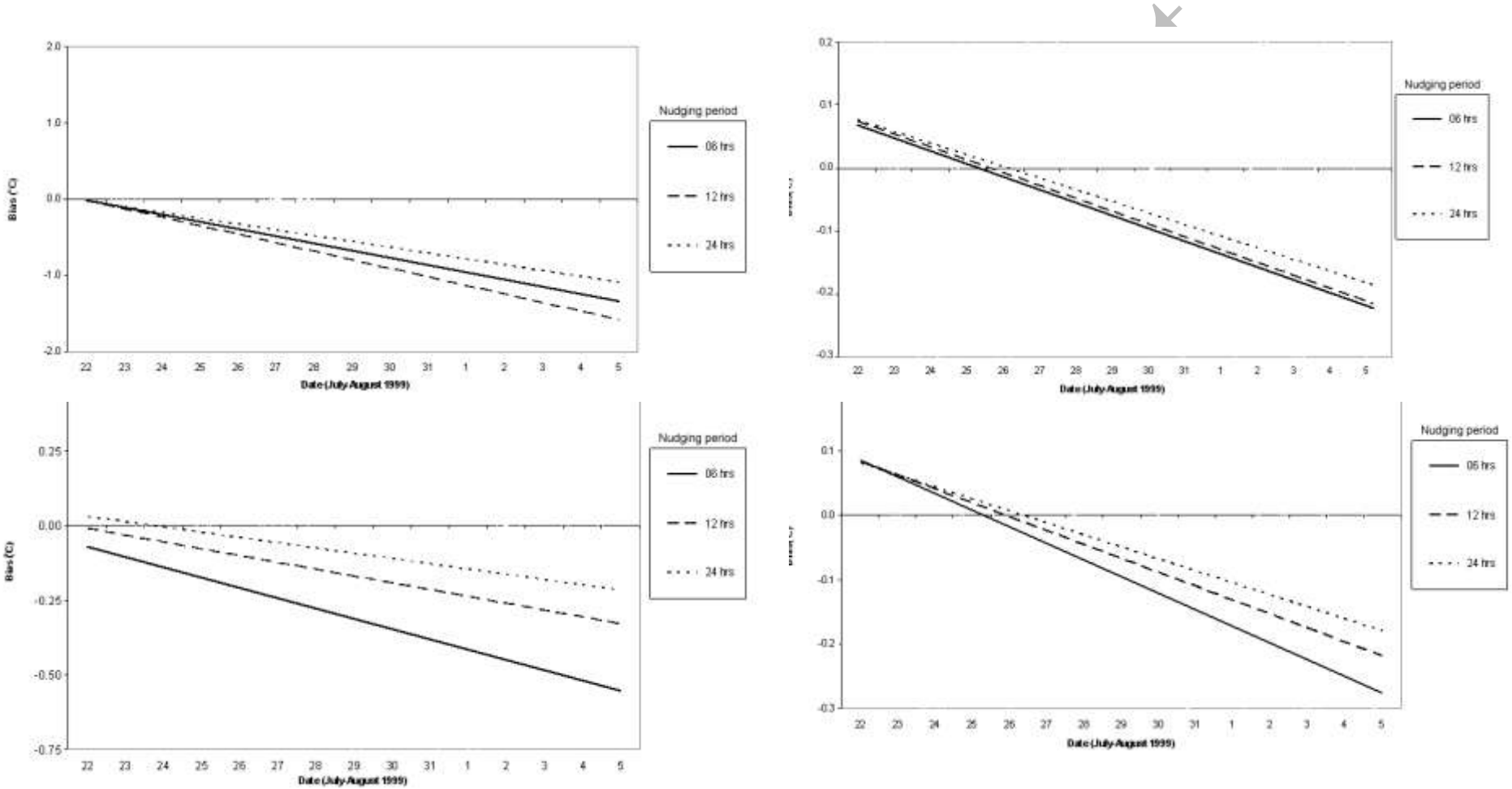

Figure 7a-d. Bias trend between the SST forecasts produced by the ocean model with using a nudging coefficient of (a) $5x10^{-3}$ (b) $5x10^{-4}$ (c) $5x10^{-5}$ and (d) $5x10^{-6}$ with different nudging periods.

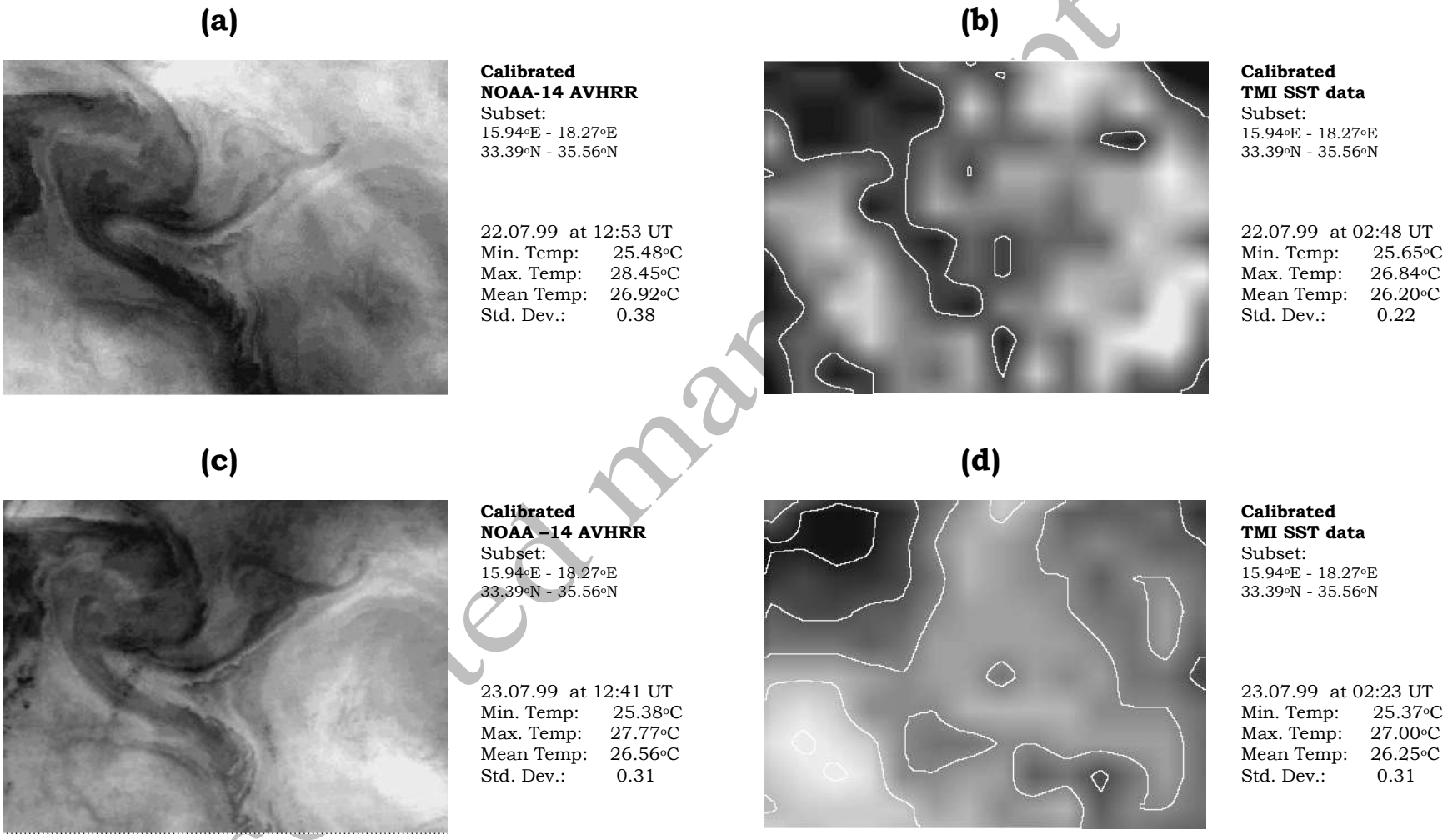

Figure 8 a-d. An overview of some datasets used to initialise, nudge, and verify the predicted oceanic fields. The thermal profiles (a) and (c) were retrieved by the NOAA AVHRR sensor on the 22nd and 23rd July 1999. (Dark fields denote colder and lighter fields denote warmer surface water). The thermal profiles (b) and (d) were retrieved by the passive microwave TMI sensor. In spite of the coarser detail identified by the TMI sensor, the thermal signature is still evident (aided by contours), where major filaments originating from the cold core are evident.

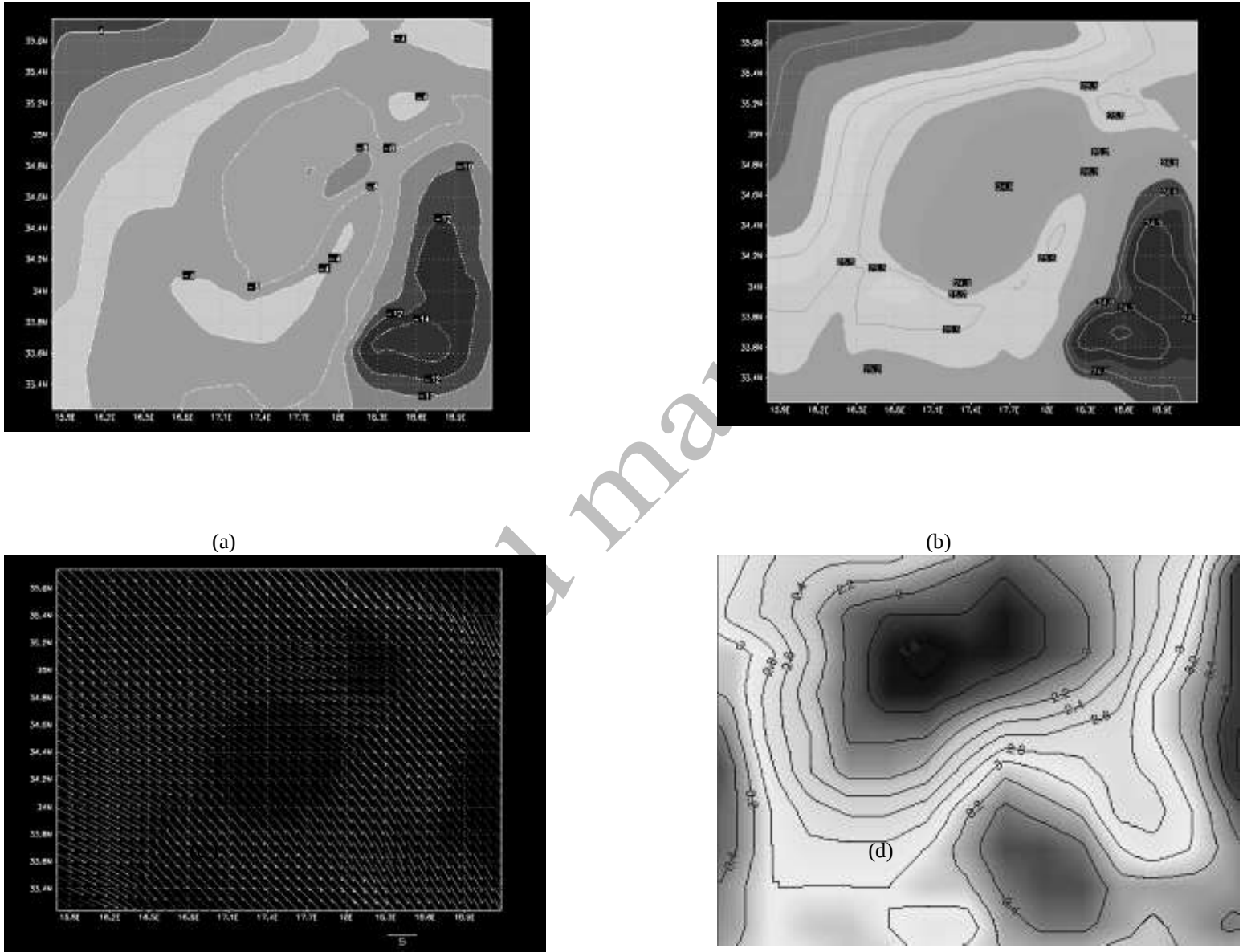

(a) (b)

(d)

Figure 9 a-d. Predicted and observed fields on 23.07.99 at 00:00 UT. The sensible heat flux (a) corresponds to the predicted 2 m air temperature (b), and the predicted (c) and observed (d) 10 m wind magnitude (ms^{-1}).

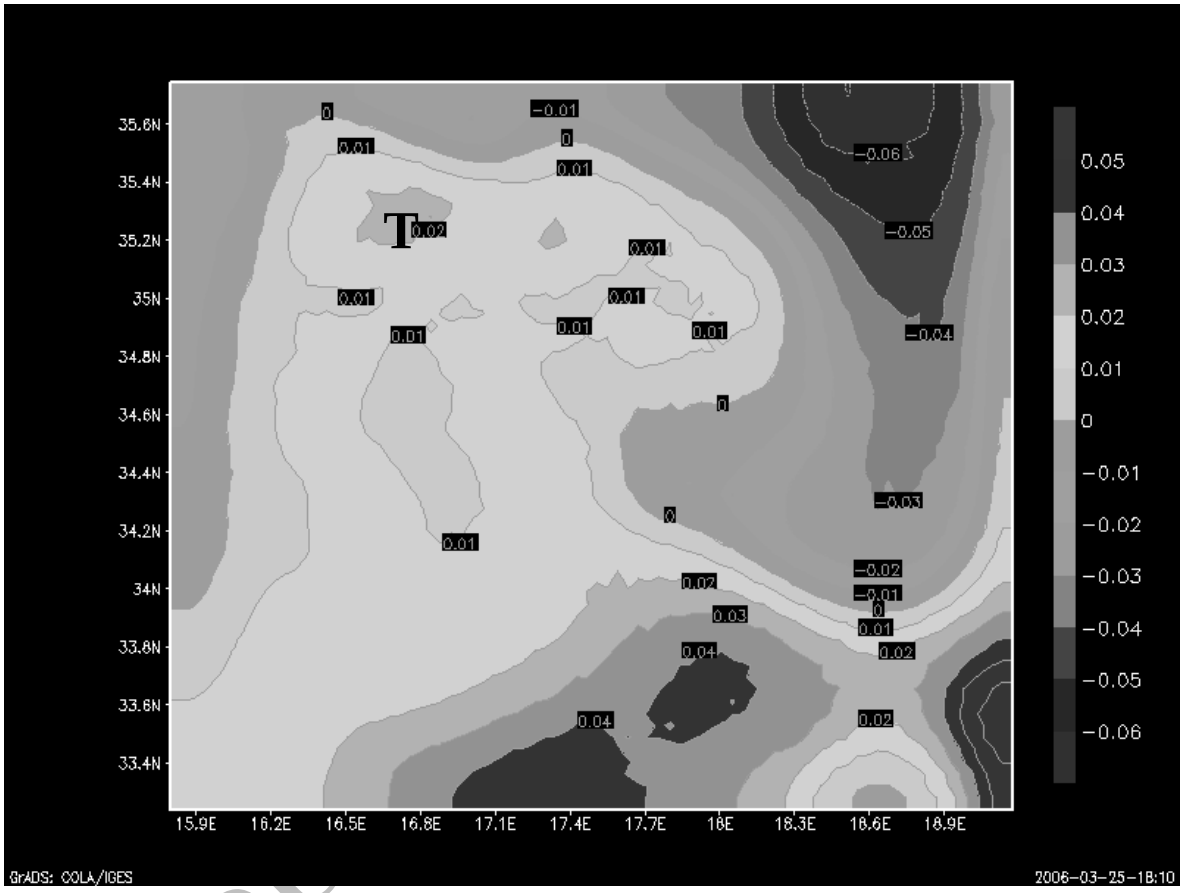

Figure 10. 12-hour forecast of the sea surface elevation (m) predicted by the ocean model (using DA scheme 1; τ=24 hours; experimental air-sea fluxes) starting at 22.07.99 00 UT. The surface flow is characterised by a stable, slightly elevated sea surface.

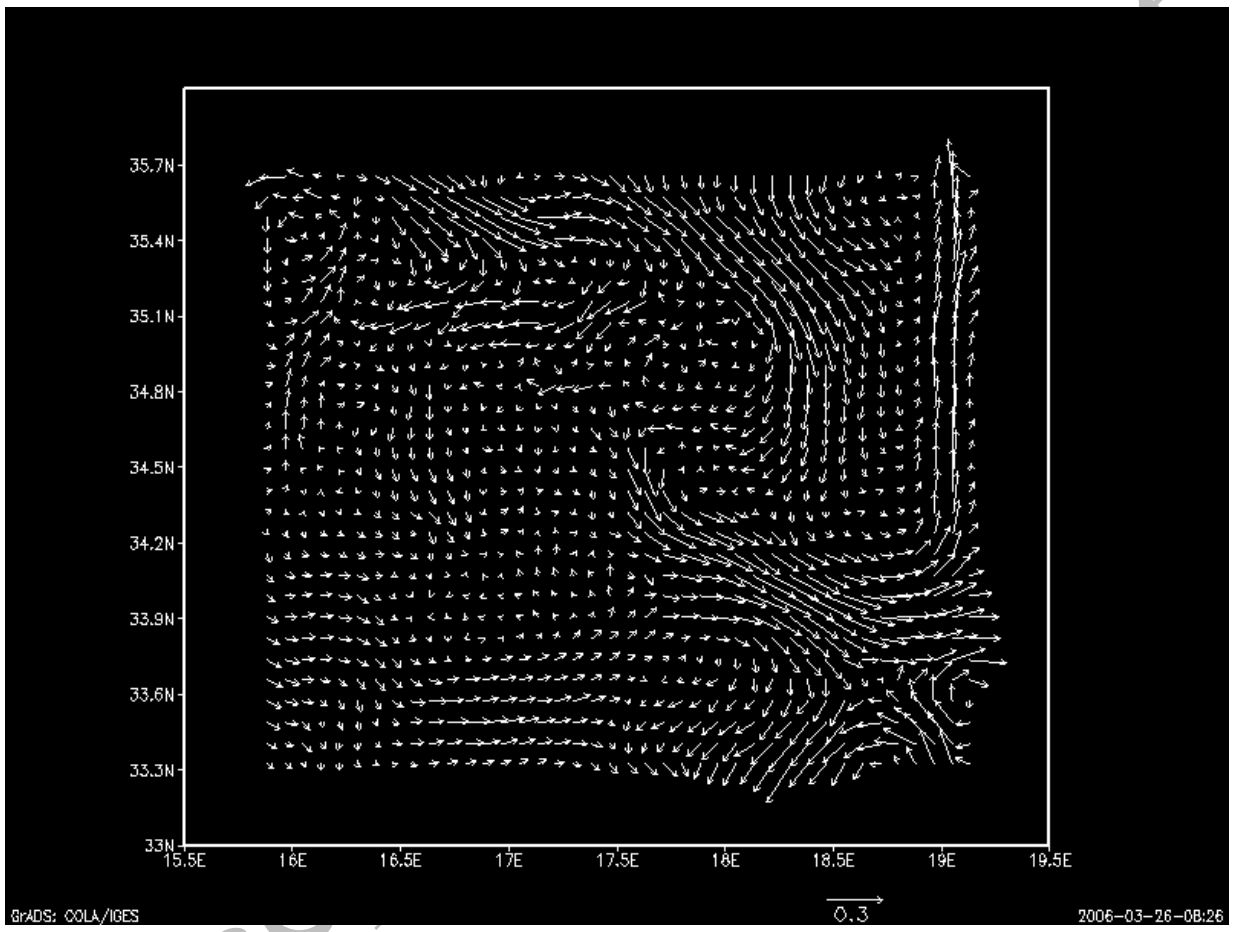

Figure 11. Direction and magnitude (cm s^{-1}) of the surface ocean currents as predicted at the 36th hour from the start of the model integration on the 22nd of August 1999 at 00 UT. TMI-SST was assimilated in the ocean model using DA scheme 1 with a τ = 24 hrs. (Scale arrow is 0.3 cm s^{-1}).

Figure 12 a-c. SST features as (a) retrieved by AVHRR on the 23rd July 1999 at 12:41 UT , (b) predicted SST field for 23rd July 1999 at 12:00 UT (using DA scheme 1; τ=24 hours), and (c) retrieved by TMI sensor on the 24th July 1999 at approximately 00 UT.

A=cool vortex; B=cool filament; C=warmer pool; D & E= temperature gradients.

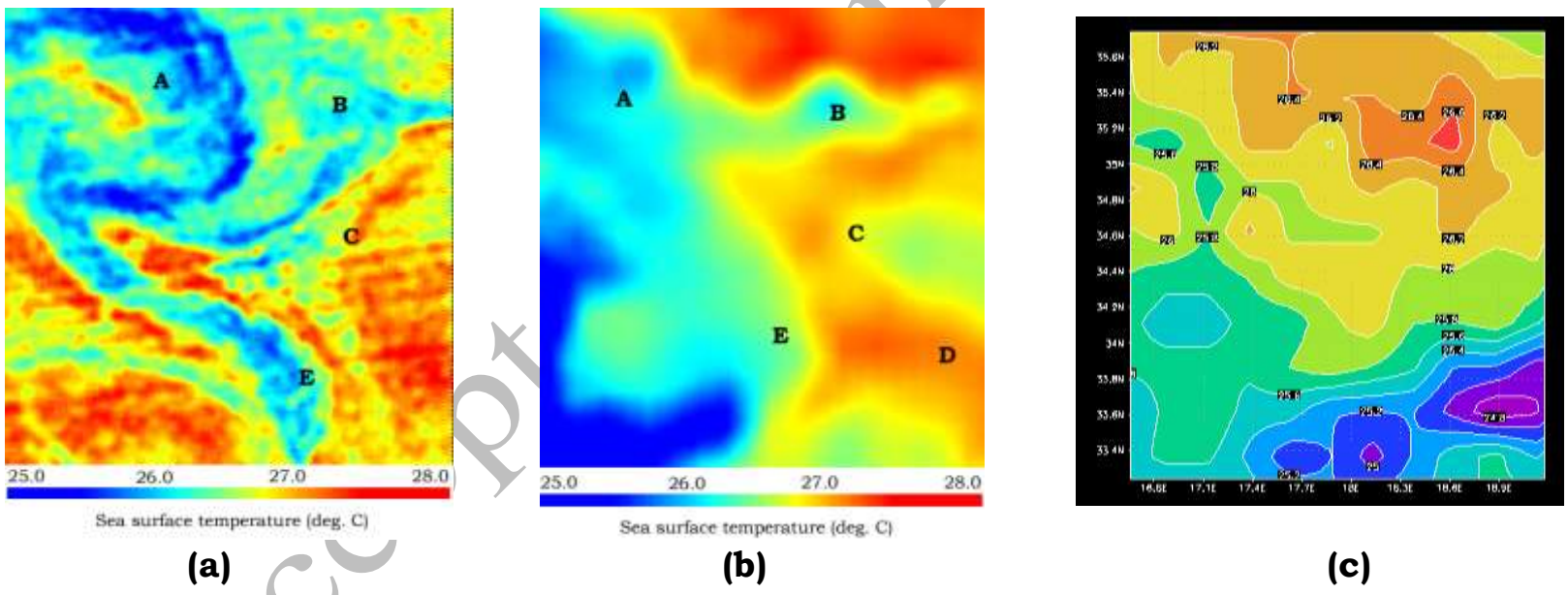

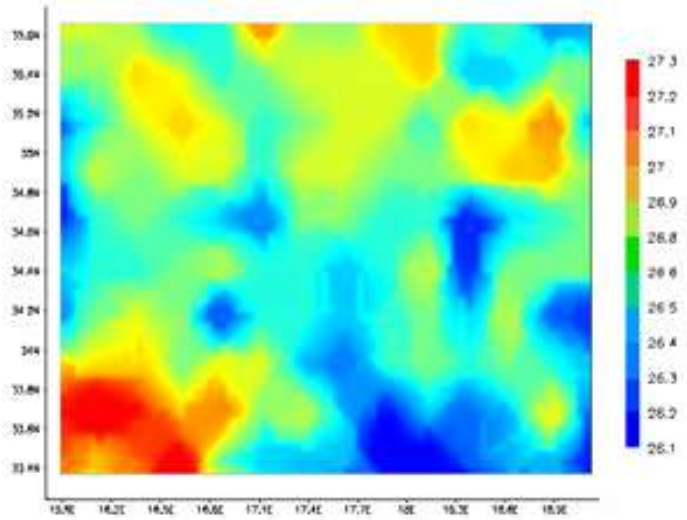

TMI-derived SST (in °C)
on 04.08.99 @ 21.7 UT.
This was
used to nudge model variables
during the pre-forecast run.

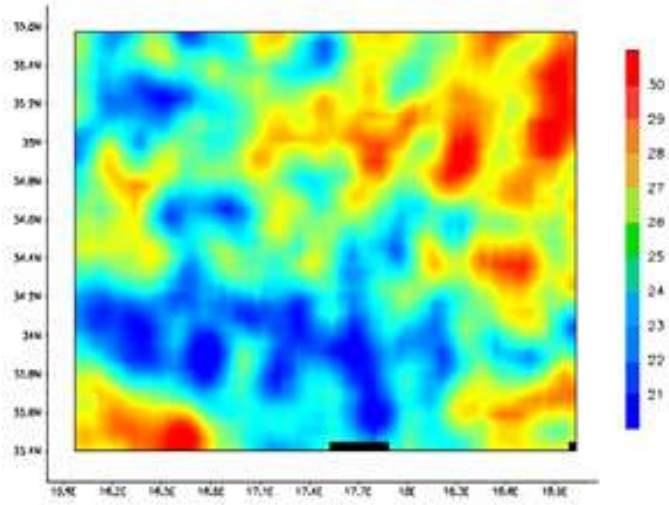

Final forecasted SST field (in °C)
on 06.08.99 @ 00 UT.
Coefficient value=$5x10^{-4}$;
τ=06 hrs

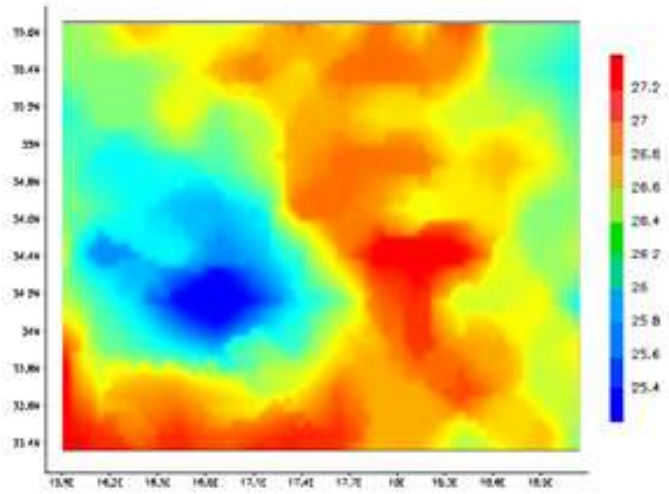

TMI-derived SST (in °C)
on 05.08.99 @ 21 UT.

Figure 13 a-c. Model predicted SST on 6th August at 00 UT using the optimal settings identified for the data assimilation using TMI-derived SST and the set of air-sea fluxes predicted by the atmosphere model to drive the underlying ocean model.

Table 1. Cloud- and aerosol-free, valid geographical sectors (shaded in gray) from the South East coast area of the US. Visible and IR data from these sectors were retrieved during 1998 and 1999.

Date	Image ID	*SECTOR* A'	B'	C'	A	B	C	D	E	F	G	H	I	J	K	L	M	N	O	P	Q	R	S	T
1998																								
Feb_18	908												■	■					■					
Feb_18	910													■	■				■		■	■		
Feb_18	922													■										
Feb_19	008				■	■		■	■				■	■		■	■							
Feb_19	012							■	■	■			■	■	■				■	■	■			
Feb_20	123							■	■				■	■	■				■					
Feb_20	207							■	■				■	■					■					
Feb_20	211				■				■	■	■		■	■	■				■	■				
Feb_20	222							■	■				■	■	■				■					
Feb_21	207							■	■				■	■					■					
Feb_21	211				■				■	■	■		■	■	■				■	■				
Feb_21	222							■	■				■	■	■				■					
Feb_25	608				■			■	■				■	■					■	■				
Feb_25	611				■			■	■				■	■	■				■	■	■			
Mar_14	307		■		■				■						■						■			
Mar_15	408				■			■	■	■			■	■	■				■	■	■			
Apr_13	308	■	■	■	■	■		■	■				■	■	■									
May_16	607	■	■	■	■	■		■	■	■	■	■		■	■	■	■	■		■	■	■	■	
Jun_03	407	■	■		■	■		■	■	■	■	■	■	■	■	■	■			■				
Aug_23	507		■		■	■	■	■	■	■	■	■												
Sep_05	808	■	■	■	■	■							■	■	■	■	■		■	■	■	■	■	
Nov_28	208	■	■	■	■	■	■	■	■	■	■	■	■	■	■	■	■	■	■	■	■			
1999																								
Jan_19	1908		■						■						■				■					
Mar_17	600		■		■		■	■	■		■	■	■	■	■	■	■	■	■	■	■	■	■	■
Mar_17	607	■	■		■		■	■	■		■			■	■	■	■	■		■	■	■		
Mar_23	208		■					■	■	■			■	■	■	■			■					■
Mar_29	808				■	■		■	■	■	■	■			■	■					■			
Mar_30	900																			■	■			
Apr_14	400		■		■	■							■						■					
Nov_07	100		■		■	■	■	■	■	■	■	■	■	■	■	■	■		■	■	■	■		
Nov_07	108				■	■		■	■	■			■	■	■	■			■	■	■	■		

Table 2. Details of individual AVHRR LAC scenes, including data integrity, collected over the central Mediterranean during the period 20 July – 7 August 1999. Source: Satellite Active Archive – NESDIS.

Image	Sat/Orbit no.	Date	Time (UT)	Data Integrity over domain
N14/NSS.LHRR.NJD99201.S1415.E1427.B234	LAC/23466	Jul 20 1999	13:15:55	no contamination
N14/NSS.LHRR.NJD99202.S1404.E1415.B234	LAC/23480	Jul 21 1999	13:04:29	no contamination
N14/NSS.LHRR.NJD99203.S1353.E1404.B234	LAC/23494	Jul 22 1999	12:53:00	no contamination; presence of dust aerosols over Gulf of Gabbes moving eastwards
N14/NSS.LHRR.NJD99204.S1352.E1352.B235	LAC/23508	Jul 23 1999	12:41:33	no contamination; presence of dust aerosols
N14/NSS.LHRR.NJD99205.S1330.E1341.B235	LAC/23522	Jul 24 1999	12:30:10	presence of dust aerosols and cloud coverage
N14/NSS.LHRR.NJD99206.S1318.E1330.B235	LAC/23536	Jul 25 1999	12:18:40	presence of extensive dust aerosols and cloud coverage
N14/NSS.LHRR.NJD99207.S1307.E1318.B235	LAC/23550	Jul 26 1999	12:07:25	presence of dust aerosols and cloud coverage
N14/NSS.LHRR.NJD99208.S1255.E1307.B235	LAC/23564	Jul 27 1999	11:55:58	presence of dust aerosols and extensive cloud coverage
N14/NSS.LHRR.NJD99209.S1244.E1255.B235	LAC/23578	Jul 28 1999	11:42:22	presence of extensive cloud coverage
N14/NSS.LHRR.NJD99210.S1455.E1426.B235	LAC/23593	Jul 29 1999	13:15:11	presence of extensive cloud coverage
N14/NSS.LHRR.NJD99211.S1403.E1414.B236	LAC/23607	Jul 30 1999	13:03:29	presence dust aerosols and clouds
N14/NSS.LHRR.NJD99212.S1352.E1403.B236	LAC/23621	Jul 31 1999	12:52:09	presence of cloud coverage
N14/NSS.LHRR.NJD99213.S1340.E1352.B236	LAC/23635	Aug 01 1999	12:40:35	presence of dust aerosols and cloud coverage
N14/NSS.LHRR.NJD99214.S1329.E1340.B236	LAC/23649	Aug 02 1999	12:29:07	presence of dust aerosols and extensive cloud coverage
N14/NSS.LHRR.NJD99216.S1306.E1317.B236	LAC/23677	Aug 04 1999	12:06:16	presence of cloud coverage
N14/NSS.LHRR.NJD99217.S1254.E1306.B236	LAC/23691	Aug 05 1999	12:54:53	presence of extensive cloud coverage
N14/NSS.LHRR.NJD99218.S1243.E1254.B237	LAC/23705	Aug 06 1999	11:43:31	extensive cloud coverage; partial satellite coverage over area of interest
N14/NSS.LHRR.NJD99219.S1229.E1236.B237	LAC/23719	Aug 07 1999	11:29:04	no satellite coverage over area of interest

Table 3a. Table containing the suite of single line equations valid for different atmospheric states as defined by their slopes ranging from 1.01 to 0.94. The regression analysis was done over a two-year period over the CoastWatch area. Regression models are statistically significant at the 1% level (P-value <0.01).

Month-Day	Image ID	Coast-Watch Sector	No. of pixels	Group	Regression model	Atmospheric transmittance	R-squared (adjusted for d.f.) %	Mean Absolute residual Error	No. of studentized residuals >2.0
03-15	408	A	2286	1	NLSST = 21.05 + 0.94*TB_4 - 0.65*TB_4-TB_5	$[\Delta TB_4/\Delta TB_5]$ = 1.01	99.03	0.34	645
05-16	607	M	6460	1					
05-16	607	Q	202	2	NLSST = -12.42 + 1.05* TB_4 + 1.36*TB_4-TB_5	$[\Delta TB_4/\Delta TB_5]$ = 0.98	99.92	0.09	80
03-15	408	F	6735	2					
11-28	208	L	1195	2					
03-14	307	B'	4599	3	NLSST = -3.09 + 1.01*TB_4 + 1.69*TB_4-TB_5	$[\Delta TB_4/\Delta TB_5]$ = 0.97	99.96	0.12	244
09-05	N/a	P	1064	3					
11-28	208	C	205	3					
04-13	308	A'	5317	4	NLSST = -25.57 + 1.10*TB_4 - 0.83*TB_4-TB_5	$[\Delta TB_4/\Delta TB_5]$ = 0.96	93.96	0.29	735
04-13	308	B'	5940	5	NLSST = -10.22 + 1.04*TB_4 + 1.14*TB_4-TB_5	$[\Delta TB_4/\Delta TB_5]$ = 0.95	99.90	0.12	892
04-13	308	C'	4972	5					
11-28	208	C'	1756	5					
03-15	408	J	5072	6	NLSST = 3.61 + 0.99*TB_4 + 1.56*TB_4-TB_5	$[\Delta TB_4/\Delta TB_5]$ = 0.94	99.76	0.16	999
03-15	408	K	792	6					
04-13	308	B	4512	6					
04-13	308	J	6469	6					
05-16	607	B'	6365	6					
05-16	607	G	894	6					

Table 3b. Table containing the suite of single line equations valid for different atmospheric states as defined by their slopes ranging from 0.93 to 0.86. The regression analysis was done over a two-year period over the CoastWatch area. Regression models are statistically significant at the 1% level (P-value <0.01).

Month	Image ID	Coast-Watch Sector	No. of pixels	Group	Regression model	Atmospheric transmittance	R-squared (adjusted for d.f.) %	Mean Absolute Error	No. of studentized residuals >2.0
04-13	308	K	6282	7	$NLSST = -17.22 + 1.06*TB_4 + 1.53*TB_4-TB_5$	$[\Delta TB_4/\Delta TB_5] = 0.93$	99.81	0.11	477
11-28	208	B	1277	7					
11-28	208	M	965	7					
04-13	308	A	3559	8	$NLSST = -16.00 + 1.06*TB_4 + 0.87*TB_4-TB_5$	$[\Delta TB_4/\Delta TB_5] = 0.92$	99.25	0.25	1123
05-16	607	N	6599	8					
06-03	407	A'	5533	8					
06-03	407	K	1957	8					
11-28	208	J	5274	8					
11-28	208	K	2849	8					
11-28	208	O	1987	8					
05-16	607	F	1499	9	$NLSST = -2.22 + 1.01* TB_4+ 1.85*TB_4-TB_5$	$[\Delta TB_4/\Delta TB_5] = 0.91$	99.70	0.11	281
06-03	407	B'	4009	9					
03-15	408	P	402	10	$NLSST = 12.71 + 0.96*TB_4+ 1.87*TB_4-TB_5$	$[\Delta TB_4/\Delta TB_5] = 0.90$	98.93	0.14	707
06-03	407	A	5417	10					
06-03	407	B	1420	10					
11-28	208	N	4655	10					
11-28	208	P	321	10					
03-15	408	O	3757	11	$NLSST = -9.20 + 1.03*TB_4 + 1.56*TB_4-TB_5$	$[\Delta TB_4/\Delta TB_5] = 0.89$	99.73	0.12	437
05-16	607	C	636	11					
05-16	607	C'	5460	11					
03-15	408	I	4389	12	$NLSST = -21.93 + 1.08*TB_4 + 0.04*TB_4-TB_5$	$[\Delta TB_4/\Delta TB_5] = 0.87$	99.39	0.25	432
05-16	607	R	2707	12					
05-16	607	B	3113	13	$NLSST = -10.88 + 1.04*TB_4 + 1.14*TB_4-TB_5$	$[\Delta TB_4/\Delta TB_5] = 0.86$	99.62	0.09	117

Date	algorithm	SST Field (°C)				remarks
20-Jul-99		**mean**	**maximum**	**minimum**	**Standard deviation**	
	Coll94	27.25	30.74	25.56	0.78	
	Regression model	27.02	30.38	25.39	0.75	$\Delta TB_4/\Delta TB_5$ =1.1; group 2
	TMI	26.23	27.10	24.82	0.44	
21-Jul-99		**mean**	**max**	**min**	**stdev**	
	Coll94	27.17	30.08	25.82	0.49	
	Regression model	25.55	27.25	24.23	0.30	$\Delta TB_4/\Delta TB_5$ =0.8; group 22
	TMI	25.92	26.40	24.92	0.25	
22-Jul-99		**mean**	**max**	**min**	**stdev**	
	Coll94	26.90	28.23	25.42	0.33	
	Regression model	26.99	28.37	25.56	0.35	$\Delta TB_4/\Delta TB_5$ =0.7; group 23
	TMI	26.20	26.85	25.52	0.30	
01-Aug-99		**mean**	**max**	**min**	**stdev**	
	Coll94	29.51	31.0	27.61	0.67	
	Regression model	28.43	29.72	26.72	0.61	$\Delta TB_4/\Delta TB_5$ =1.1; group 2
	TMI	27.29	28.92	26.43	0.52	

Table 4. Performance of linear regression models for valid AVHRR scenes over the area of interest against microwave-derived SST and the mid-latitude algorithm derived by Coll et al., (1994).